THE JOURNAL OF PHYSICAL CHEMISTRY B

Article

pubs.acs.org/JPCB

Molecular Dynamics Study on the Growth of Structure I Methane Hydrate in Aqueous Solution of Sodium Chloride

Yen-Tien Tung, Li-Jen Chen, Yan-Ping Chen, and Shiang-Tai Lin*

Department of Chemical Engineering, National Taiwan University, Taipei 10617, Taiwan

ABSTRACT: The structure, thermodynamic, and kinetic properties of methane hydrates formed from the aqueous solution of sodium chloride are investigated based on molecular dynamics simulations. A three-phase molecular model consisting of a slab of methane hydrate phase, a slab of liquid water containing sodium chloride, and a gas phase of methane molecules is used. The decrease in the three-phase coexisting temperatures (by 2−3 K) at different pressures (10−100 MPa) for aqueous NaCl solutions (about 2 mol %) confirms the thermodynamic inhibition of NaCl. The growth rate of methane hydrates in NaCl solution is found to be half to one-third of that in pure water. The kinetic inhibition of NaCl is found to be a result of the reduced water repelling at the growing interface due to the strong hydration of ions. Individual ions or NaCl ion pairs can replace water molecules to participate in the formation of the cage structures. The distortion of water cages due to the presence of ions may result in a reduced fraction of occupation of methane in the cage cavities. Our results provide useful insights into the mechanism of growth of methane hydrates in seawater and the desalination.

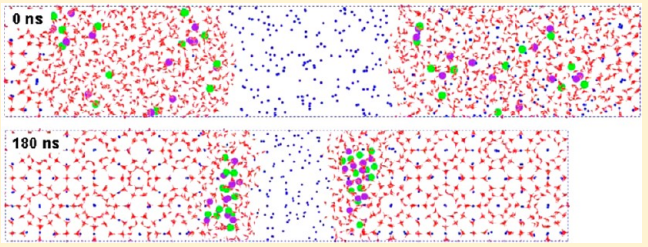

1. INTRODUCTION

Clathrate hydrates are one of the gas inclusion crystals where water molecules form the cage framework by hydrogen bonding to encapsulate small, guest molecules such as methane or carbon dioxide.[1] There is a tremendous amount of methane trapped in the form of methane hydrates all around the world (mostly in the seafloor or permafrost regions). Therefore, methane hydrates are considered as a potential energy source for the future.[2] Understanding the growth of methane hydrates in the natural environments can help their exploration and exploitation.

Molecular dynamics (MD) simulations are one of the powerful tools to study the nucleation, growth, and melting of methane hydrate;[3] however, most of them are done without the presence of sodium chloride, one of the major components in seawater. Sodium chloride is known as a thermodynamic inhibitor that increases the equilibrium pressure and/or decreases the equilibrium temperature of hydrates.[4] Recently, Wu et al.[5] reported a study on the change of crystalline structure and thermodynamic stability of methane hydrate with the inclusion of sodium chloride ions. However, the study on the kinetic inhibition of methane hydrate growth is still limited. Kinetic hydrate inhibitors are known to delay the nucleation and/or the growth of the gas hydrates.[6] The presence of an inhibitor may result in the increase of a free energy barrier for the formation of initial nuclei and/or their growth to a critical size.[7] The inhibitors may preferentially adsorb onto the surface of microcrystals and interfere with the growth of gas hydrates.[8]

The purpose of this study is to understand the role of sodium chloride in the growth of methane hydrate from salt solutions using molecular dynamics simulations. We first validate our molecular models by examining the three-phase coexisting conditions from our simulation and from experiment. We then investigate the kinetic inhibition effects of NaCl in the growth of methane hydrates. Our simulation results show that NaCl ions present at the hydrate surface retard the growth of methane hydrates. Furthermore, sodium chloride can participate in the framework of water cages and alter the occupation of methane molecules in the cavities. The results are useful for a better understanding of the formation of methane hydrates in seawater and the desalination of electrolyte solutions via clathrate hydrates.

2. COMPUTATIONAL DETAILS

The three-phase model, as shown in Figure 1, consisting of a methane gas, a liquid sodium chloride solution, and a hydrate phase is used in this study. The methane gas phase contains 160 methane molecules, and the hydrate phase consists of a $1 \times 2 \times 2$ unit cell of structure I (sI) crystalline hydrate with all its cavities (both inside and at the surface) filled with methane (i.e., 184 water molecules and 44 methane molecules). [Note that the sI unit cell contains 46 water molecules, 6 large $5^{12}6^2$ cavities, and 2 small 5^{12} cavities]. The structure crystalline hydrate is created following the Bernal−Fowler ice rule.[9] Two liquid solution slabs are placed between the gas and solid phases: one liquid solution slab with the sodium chloride concentration of seawater (736 water molecules, 12 chloride ions, and 12 sodium ions (5 wt % or 1.6 mol %), on the RHS of the solid phase in Figure 1) and one liquid solution slab with the same sodium chloride concentration and supersaturated with methane (736 water molecules,

Received: August 18, 2012
Revised: October 28, 2012
Published: November 8, 2012

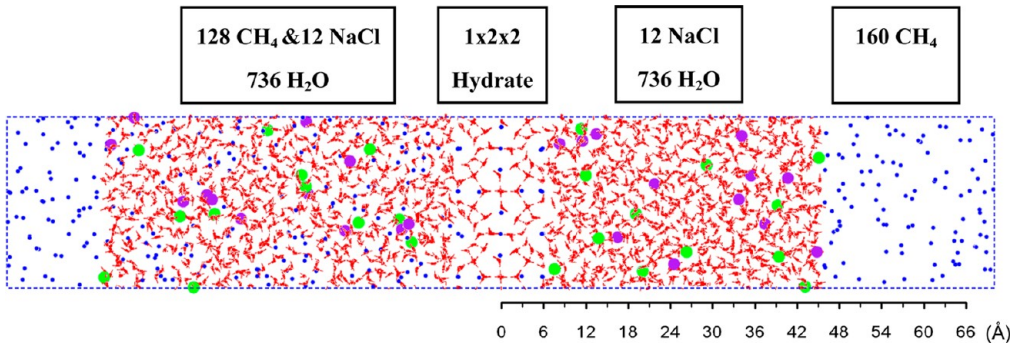

Figure 1. Initial molecular structure of a three-phase methane hydrate model. The model consists of a 1 × 2 × 2 structure I hydrate slab (in the middle), two liquid solution slabs (on the right-hand side is a sodium chloride aqueous solution, and on the left-hand side is the solution with dissolved methane), and a vapor methane slab (mostly methane gas). Carbon atoms are shown in blue, oxygen in red thick sticks, hydrogen in normal sticks, chloride ions in green, and sodium ions in purple. A scale bar shown below the figure indicates the size of the model.

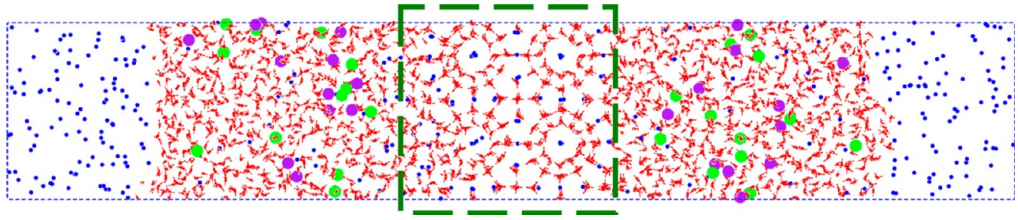

Figure 2. Initial structure used in the measurement of three-phase equilibrium temperatures. The solid phase is emphasized in the rectangular area of green dashed lines.

12 chloride ions, 12 sodium ions, and 128 methane molecules, on the LHS of the solid phase in Figure 1). Note that the methane concentration in the latter solution slab is the same as that of sI methane hydrate, which is above the methane solubility in water. The high methane concentration slab may serve as a buffer region for methane in the dynamic simulations. The size of such an initially created model (using molecular simulation package Cerius2[10]) is 137.00 Å × 23.74 Å × 23.74 Å.

The TIP4P-Ew[11] (for water) and OPLS-AA[12] (for methane) force fields are chosen to describe the interactions within the molecular model. The TIP4P force field has been used to study the gas hydrate systems.[3a−c,f,g,13] For chloride and sodium ions, we choose the OPLS of ions[14] and Åqvist[15] force fields to describe their interactions, respectively. The set of ion force field is used to successfully study the effect of salt in the ice systems.[16] The atomic charge and Lennard-Jones (LJ) interaction ($V(r) = 4\varepsilon[(\sigma/r)^{12} - (\sigma/r)^6]$) parameters can be found in the literature.[3a,14,15] The geometric combination rule ($\varepsilon_{ij} = (\varepsilon_{ii}\varepsilon_{jj})^{1/2}$ and $\sigma_{ij} = (\sigma_{ii}\sigma_{jj})^{1/2}$) is used for the LJ parameters between different types of atoms, except that σ = 3.032 Å and ε = 0.255 kcal/mol (obtained by fitting to the QM calculated interactions by Cao et al.[17]) are used for O (of water) and C (of methane) interactions. Cao et al.'s methane−water potential has been shown to give better occupancy numbers, and it can be directly used in our set of force field, TIP4P-Ew and OPLS-AA. All the subsequent molecular mechanic and dynamic simulations are performed using the open source package, LAMMPS.[18] The initially created model is first energy minimized, and a short, 20 ps, NVT simulation at 200 K is performed to relax any extra stress at the solid−liquid and the liquid−gas interfaces. The relaxed system is then heated from 200 to 260 K at a rate of 0.5 K/ps under constant pressure. Finally, the system is subjected to long (for up to 140 ns, mostly for 40 ns) NPT simulations for the study of methane hydrate growth. The pressure effect is studied by using four sets of simulations at pressures of 10, 30, 60, and 100 MPa, respectively. The periodic boundary condition is applied to the simulation box in all three directions. The Nose-Hoover temperature thermostat[19] with the relaxation time of 0.1 ps and pressure barostat[20] with the relation time of 1 ps are used.[21] The integration time step is set to 1 fs. In our NPT simulations, two independent barostats with the same target pressure are used, one for the normal stress in the x direction (the growth direction, see Figure 1) and the second for the y and z directions. The Lennard-Jones potential energy is calculated with a cutoff of 9.5 Å (around three times σ of the O atom), and the long-range Coulomb energy is calculated by PPPM[22] with a cutoff of 8.5 Å for the real part calculation. Three independent simulations (using different random seeds for velocity initialization) are performed at each temperature and pressure condition to obtain the statistics of properties.

Table 1. Three-Phase (Hydrate−Solution−Vapor) Coexisting Temperature T_m and Pressure P Determined from Molecular Dynamics Simulations

P (MPa)	T_m from MD (K)	T_m from experiment[4b] (K)	simulated temperatures (K) (simulation time in ns)
10	279 ± 1	283.6(9.6 MPa)	270(20),278(20),280(20)
30	288 ± 3	292(28 MPa)	282(20),287(20),290(20),292(20), 295(20)
60	292 ± 2	297(56 MPa)	285(20),287(20),292(20),295(20)
100	296 ± 3	–	290(20),293(20),295(20),297(20), 300(20)

The three-phase (hydrate, liquid solution, and vapor, H−L−V) coexisting equilibrium temperatures of methane hydrate in the sodium chloride solutions at the four studied pressures are

dx.doi.org/10.1021/jp308224v | J. Phys. Chem. B 2012, 116, 14115−14125

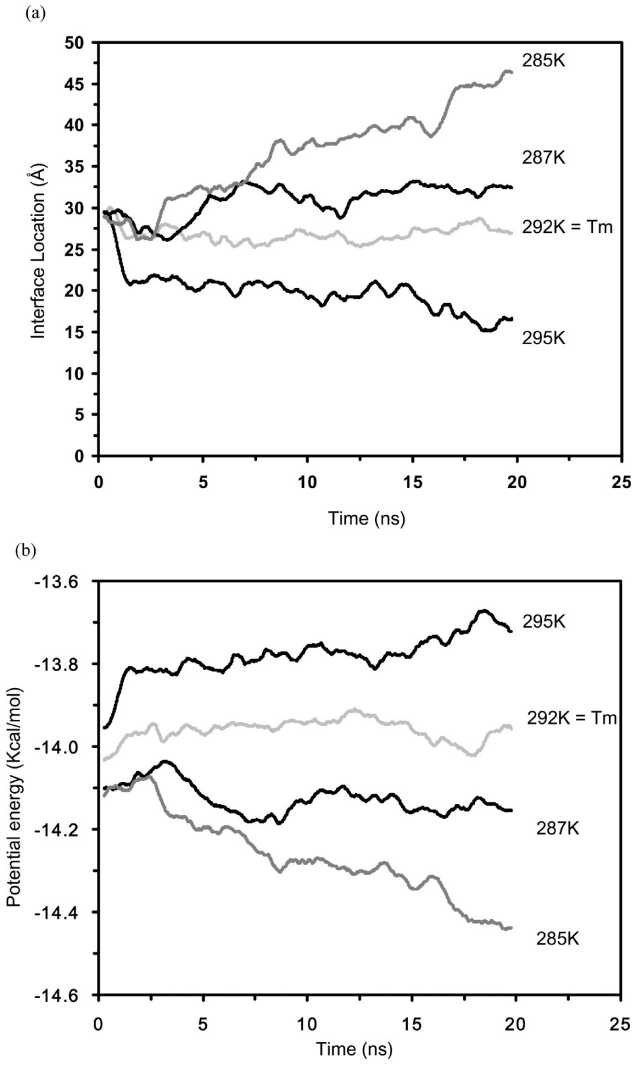

Figure 3. Time evolution of the thickness of the solid phase (a) and the potential energy (b) of the system at 60 MPa and different temperatures (285, 287, 292, and 295 K). The melting temperature (T_m) at 60 MPa is estimated to be about 292 K.

determined by performing a series of simulations at several temperatures around the melting temperature for each pressure of interest. The initial structure for such simulations is taken from an NPT simulation at 30 MPa and 260 K after 35 ns, as shown in Figure 2, where the hydrate phase is grown to a thickness of 30 Å and the concentration of NaCl is increased to about 2 mol % (or 6 wt %). The size of the initial structure is around 136.9 Å × 23.7 Å × 23.7 Å. All simulation parameters are the same as those used for the growth study described previously. At a desired pressure, the temperature of the initial structure is increased to the desired value from 260 K at a rate of 0.5 K/ns. Subsequent NPT simulations are performed for up to 20 ns, and the thickness of the hydrate phase is examined. The simulations performed are summarized in Table 1.

The angular order parameter (AOP) of a water molecule defined in eq 1 below is used to identify the structural characteristic of water configuration.[23]

$$\mathrm{AOP} = \sum [(|\cos\theta|\cos\theta) + \cos^2(109.47^0)]^2 \quad (1)$$

where θ is the inclusion angle among the oxygen atom of the water molecule of interest and any two oxygen atoms of the

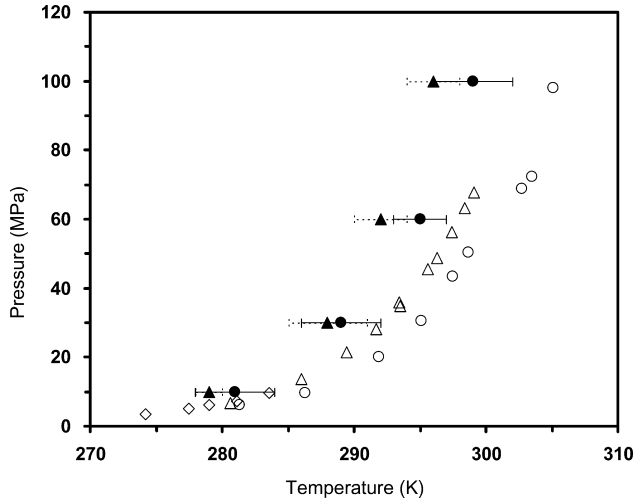

Figure 4. Comparison of the melting temperatures of methane hydrates determined by MD simulations in pure water[3a] (filled circles) and in aqueous solution of NaCl (1.7−2.3 mol %) (filled triangles). Experimental data are taken from Jager and Sloan[4b] (open circles: 0 mol % NaCl solution and open triangles: 2 mol % NaCl solution) and Richon et al.[4d] (open diamonds: 1.6 mol % NaCl solution).

neighboring water molecules. The summation runs over all possible θ of water molecules within a radius of 3.5 Å from the center oxygen atom of interest. The average AOP of ice and hydrate crystalline structure are 0[24] and 0.1, respectively, while that of liquid water (amorphous) is about 0.8. The interface between the hydrate and the liquid is defined as the location where the AOP of water is 0.4. The growth rate of hydrate is determined from the rate of the interface movement. All our simulation temperatures are above the ice melting point of TIP4P-Ew water (around 245 K[25]), and no ice structure was found in our simulations.

3. RESULTS AND DISCUSSION

3.1. Equilibrium Phase Diagram. Figure 3(a) shows the changes in the thickness of the solid phase with time at different temperatures (285, 287, 292, and 295 K) and 60 MPa. It can be seen that the amount of methane hydrate increases at 287 K and decreases above 295 K. The melting/crystallization of the hydrate phase are also evidenced by the change in the potential energy of the system, as shown in Figure 3(b). The increase of potential energy (PE) at 295 K indicates melting, while the decrease of PE at 287 K indicates crystallization.[25b] At 292 K, the PE of the system fluctuates around −14.0 kcal/mol (based on the system of 1656 water molecules). On the basis of these observations, we conclude that the three-phase equilibrium temperature at 60 MPa is around 292 K. Repeating such simulations and analysis at other pressures (10, 30, and 100 MPa) gives the melting temperature as a function of pressure as summarized in Table 1 and shown in Figure 4. (Note in Table 1 that the uncertainty is estimated from the temperature difference between 287 and 295 K. Similar estimates are used to estimate the average and uncertainty at other pressures.) As can be seen in Figure 4, the melting temperature for the system with chloride and sodium ions from simulations is lower than that obtained from the system without chloride and sodium ions by about 2−3 K. The decrease in the equilibrium temperature and melting curve is in good agreement with experimental data (open triangles and diamonds). These results support that the model and force field

dx.doi.org/10.1021/jp308224v | J. Phys. Chem. B 2012, 116, 14115−14125

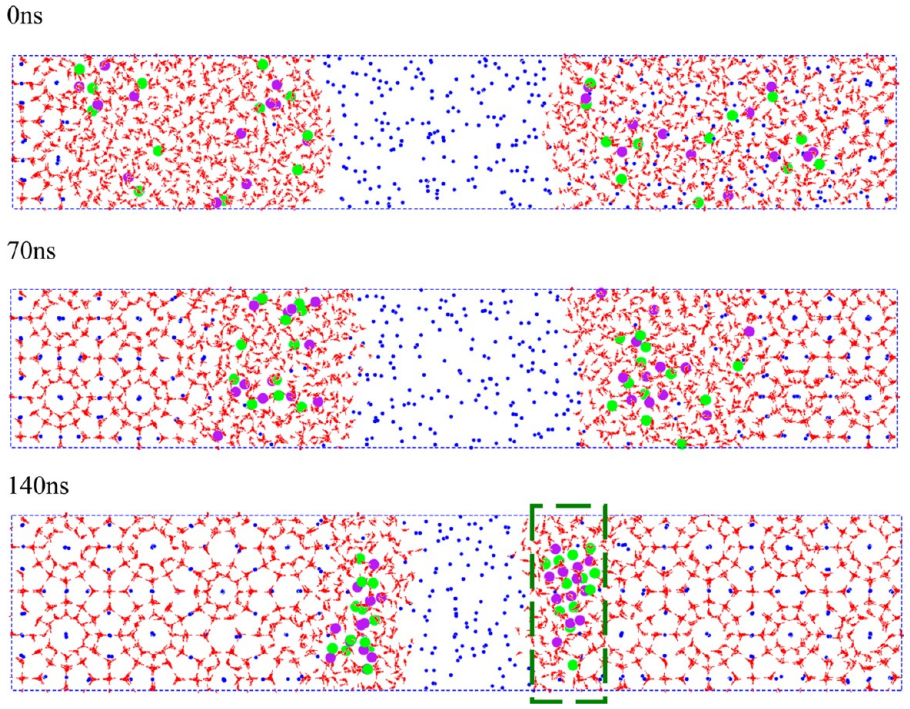

Figure 5. Snapshots taken from the methane hydrate growth simulation at 30 MPa and 260 K. The rejection of chloride and sodium ions occurs during the growth of methane hydrate, and eventually precipitation is observed at 140 ns (highlighted in the rectangular area of green dashed lines).

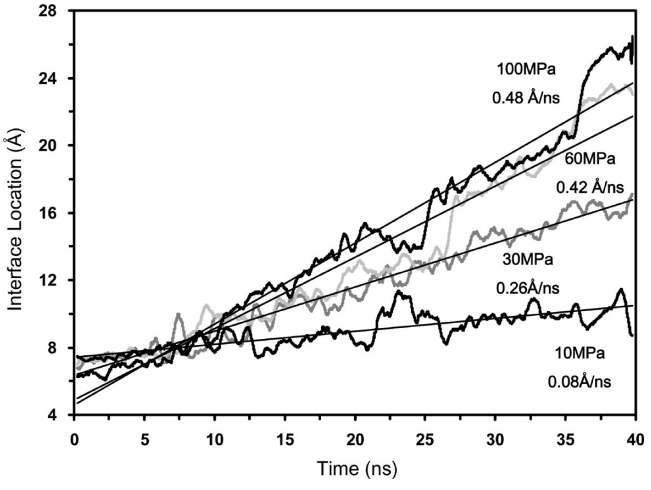

Figure 6. Time evolution of the location of solid−liquid interface from NPT simulations at 260 K and 4 pressures (10, 30, 60, and 100 MPa). The slope of these curves indicates the growth rate of methane hydrate.

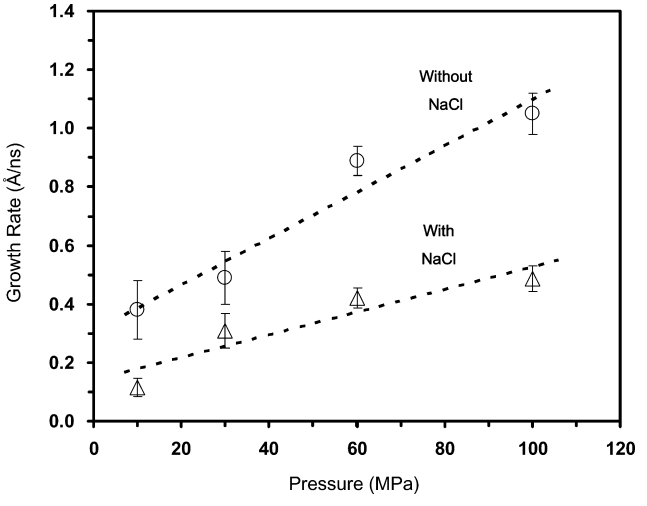

Figure 7. Comparisons of the changes in growth rates of methane hydrate with pressure at 260 K in the system without (open circles) and with sodium chloride (triangle circles). The dashed line is the best linear fit to the growth rates.

Table 2. Conditions and Simulation Time Used in the Simulations for the Growth of Methane Hydrate in the System with and without Sodium Chloride in the Liquid Phase[a]

pressure (MPa)	temperature (K)	growth rates without NaCl[3a] (Å/ns)	growth rates with NaCl (Å/ns)
10	260	0.38 (0.10)	0.12 (0.03)
30		0.49 (0.09)	0.31 (0.06)
60		0.89 (0.05)	0.42 (0.04)
100		1.05 (0.07)	0.49 (0.05)

[a]The values in the parentheses represent the statistical uncertainty.

used in this study are adequate for the study of the methane hydrate growth in aqueous salt solutions.

3.2. Growth Rate of Methane Hydrate. NPT simulations at 260 K and three pressures are conducted to study the growth of methane hydrate in the sodium chloride aqueous solution. From Figure 4, the temperature of 260 K is well within the hydrate stability region. Figure 5 illustrates the snapshots of NPT simulations at 30 MPa and 260 K. The rejection of chloride and sodium ions occurs during the growth of methane hydrate, and eventually precipitation is observed. It can be seen that the solid phase increases significantly over the time span of 70 ns. (The 0 ns is the beginning of the production simulation, which has undergone the energy minimization and a short, ~240 ps NVT and NPT equilibration simulation.) By using the angular order parameter (AOP) as an index for identifying the location of the

dx.doi.org/10.1021/jp308224v | J. Phys. Chem. B 2012, 116, 14115−14125

solid−liquid interface, the increase of thickness of the solid phase with time can be quantified, as shown in Figure 6. The slope of such curves indicates the rate of a steady growth of methane hydrate. Table 2 lists the average of growth rates of methane hydrate at different pressures with and without chloride and sodium ions in the water. Simulation results for systems without NaCl are taken from our previous study.[3a] The growth rates of methane hydrate with chloride and sodium ions in the water are found to be lower than that without the ions as shown in Figure 7. Additionally, the growth rates in the system with chloride and sodium ions slightly increase with the pressure of the system, from 0.12 Å/ns at 10 MPa to 0.49 Å/ns at 100 MPa, in comparison to the growth rate trend without chloride and sodium ions. (Note that the solubility of methane in NaCl solution is found to be equal to or slightly lower than that in pure water. For example, both are around 0.14 CH_4/H_2O.)

To better understand the reason why NaCl in the water reduces the growth rate of methane hydrate, the expelling of water molecules in the growing layer is examined. From our previous study on the growth of methane hydrate, the expelling of water molecules is an essential step for the cage formation,[3a,b] as the density of the solid phase is lower than that of the liquid phase. Figure 8 shows the evolution of water molecules in the

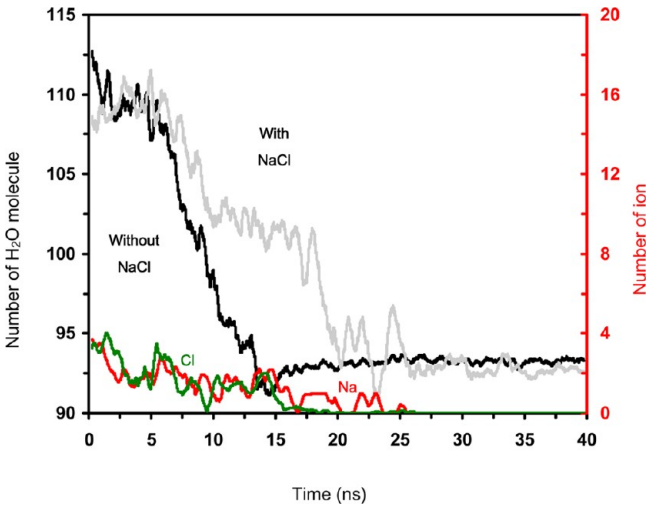

Figure 8. Time evolution of water molecules in the growing layer of 6 Å in the case without (black line) and with chloride and sodium ions (gray line), respectively, at 60 MPa and 260 K. The rate of repelling of water molecules in the case with chloride and sodium ions is found to be lower than that in the case without chloride and sodium ions.

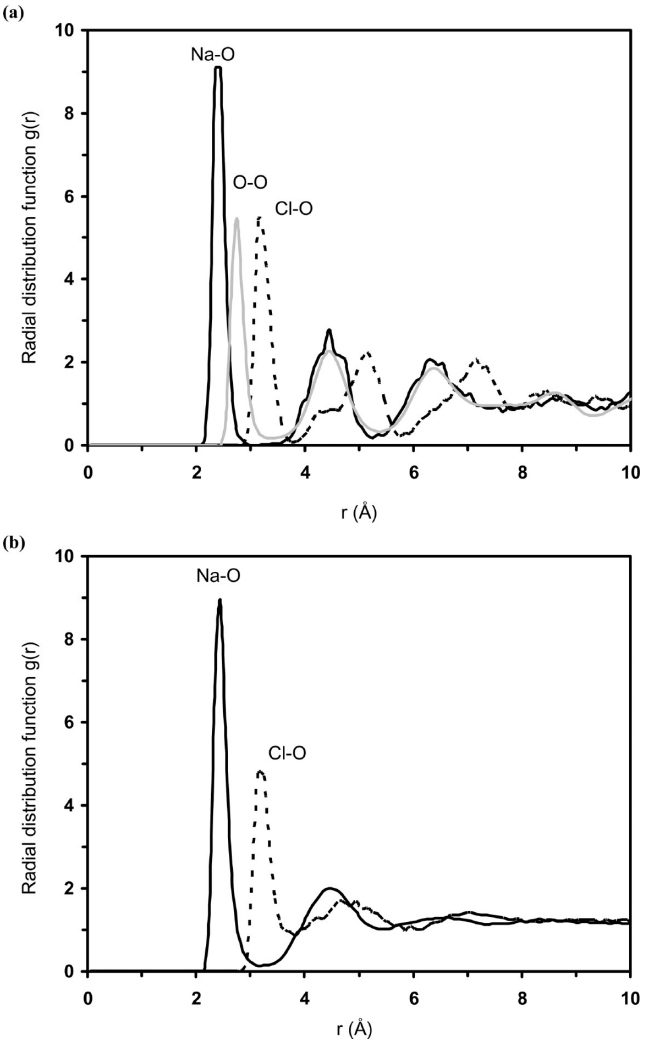

Figure 10. Radial distribution functions, $g(r)$, between chloride ions and oxygen atoms of water molecules (dashed line) and between sodium ions and oxygen atoms of water molecules (solid line) in the hydrate phase (a) and in the liquid water phase (b). The gray line represents the radial distribution function between oxygen atoms of water molecules in the hydrate phase.

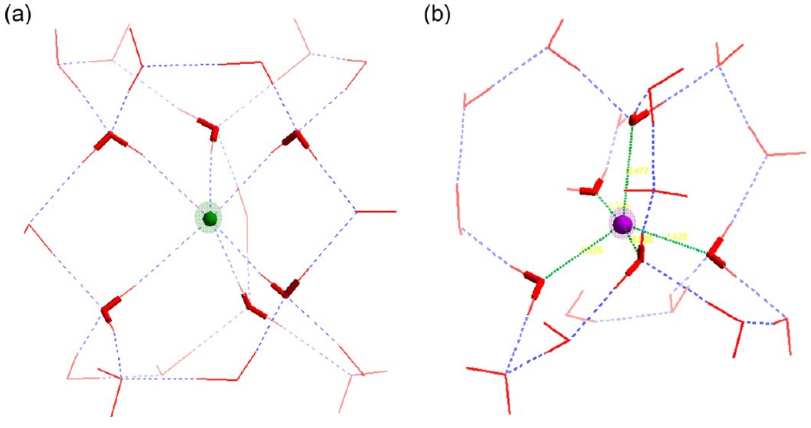

Figure 9. Water molecules around the chloride (a) and sodium ion (b) in the first hydration shell in the hydrate phase. The green and purple balls represent the chloride and sodium ions, respectively. The red cylinders are the oxygen of water molecules. The blue dashed lines represent hydrogen bonding.

dx.doi.org/10.1021/jp308224v | J. Phys. Chem. B 2012, 116, 14115−14125

growing layer of 6 Å in the case with and without sodium chloride at 60 MPa and 260 K, respectively. There are initially around 110 water molecules in this layer. When the growth of cage begins, the water molecules are repelled away from this layer, and the number of water molecules decreases to the value of 92 in the end of the growth period. From Figure 8, the repelling of water molecules in the case with chloride and sodium ions is found to be slower than that in the case without the ions. The slower repelling of water molecules indicates that the water molecules in this layer are attracted by chloride or sodium ions. In other words, the lower growth rate of methane hydrate is caused by the hydration of water molecules around ions.

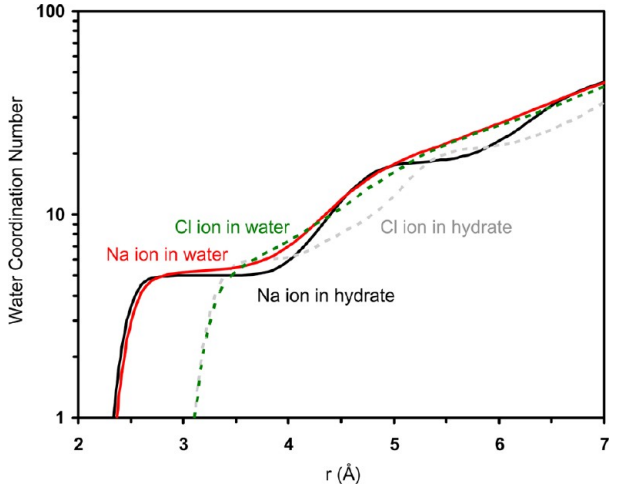

Figure 11. Water coordination number as a function of distance from the center of an ion (Na ions: solid line and Cl ions: dashed line) outward.

3.3. Inclusion of Chloride and Sodium Ions into the Cage. Desalination has been suggested as one possible application of gas hydrates. However, it has been indicated that gas hydrate grown from salt solution may not be free from salt.[5] In our simulations, we also observed the presence of sodium and chloride ions in the hydrate phase. Figure 9 illustrates the hydrated chloride and sodium ions by the cage water molecules. The chlorine ion replaces one of the cage waters and disturbs the nearby water molecules by attracting their hydrogen atoms and pushing away their equilibrium positions. The separation distance between the chloride and oxygen atom of water molecules in the hydrate phase is found to be 3.15 Å, which is larger than that between the oxygen atoms of water molecules in the hydrate phase, 2.75 Å, from the radial distribution function (Figure 10a). Similarly, as the sodium replaces one of the cage water molecules, it attracts nearby oxygen atoms and pulls them closer. The separation distance between the sodium and oxygen atoms of water molecules in the hydrate phase is found to be 2.45 Å (Figure 10b), which is less than that between the oxygen atoms of water molecules in the hydrate phase, 2.75 Å.

The hydration of sodium and chlorine ions in the hydrate phase may be a result of the similar hydration environments in the hydrate and in the liquid water phases. Figure 10b shows the radial distribution functions of ions and oxygen atoms of water molecules in the liquid water phase. The water coordination

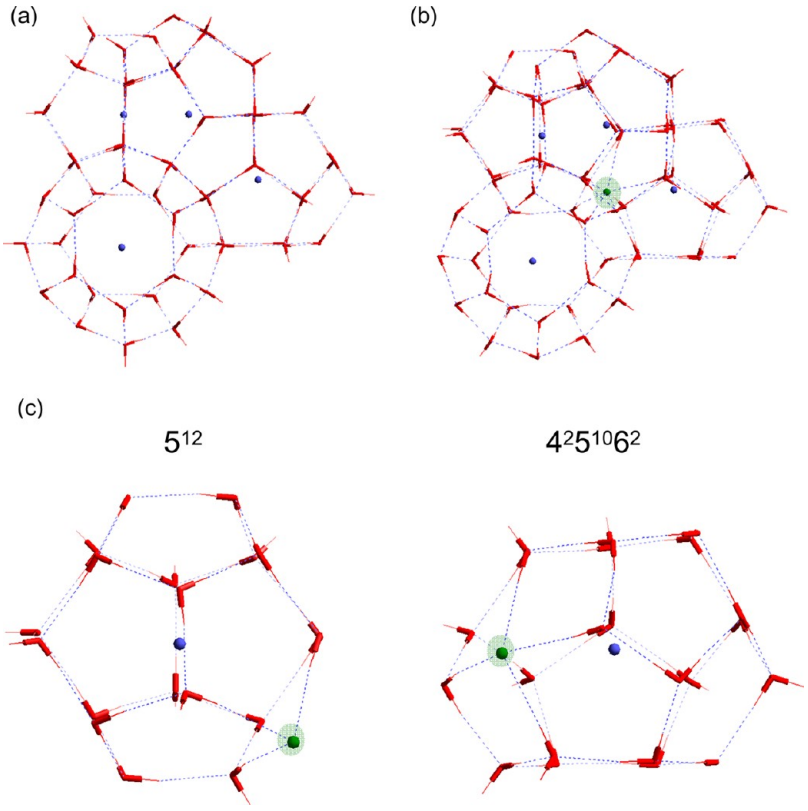

Figure 12. Comparison of the structure of stacked cages without (a) and with chloride ion (b) (type I, see text). The structure without chloride ions consists of one 5^{12} cage and three $5^{12}6^2$ cages, while the $5^{12}6^2$ cages are replaced by $4^2 5^{10} 6^2$ cages in the structure with chloride ions (c).The green and blue balls represent the chloride ions and carbon atoms of methane, respectively. The red cylinder, red stick, and the blue dashed line represent the oxygen and hydrogen atoms of water molecules and the hydrogen bonding.

dx.doi.org/10.1021/jp308224v | *J. Phys. Chem. B* 2012, 116, 14115−14125

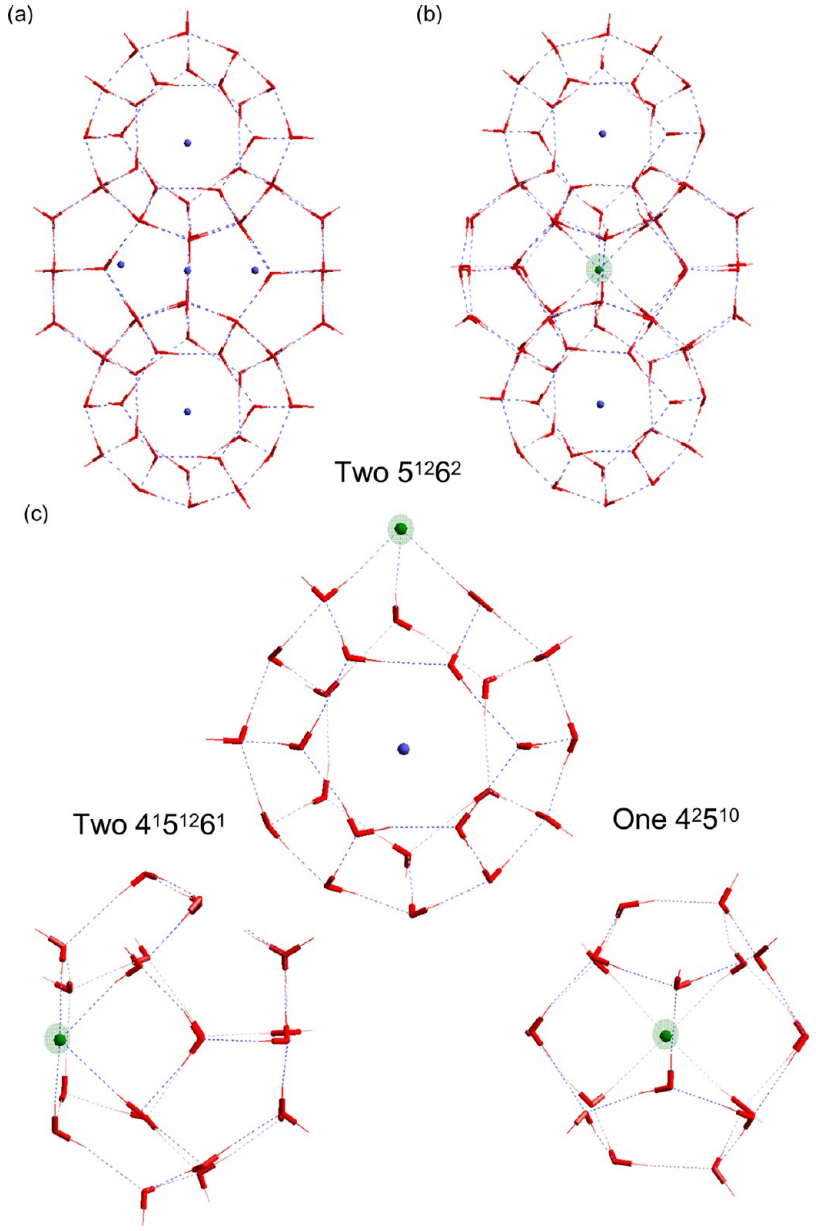

Figure 13. Comparison of the structure of stacked cages without (a) and with a chloride ion (b) (type II, see text). The structure without chloride ions consists of one 5^{12} cage and four $5^{12}6^2$ cages, while two of the $5^{12}6^2$ cages are replaced by two $4^15^{12}6^1$ cages and the 5^{12} cage is replaced by the 4^25^{10} cages in the structure with chloride ions (c). The green and blue balls represent the chloride ions and carbon atoms of methane, respectively. The red cylinder, red stick, and the blue dashed line represent the oxygen and hydrogen atoms of water molecules and the hydrogen bonding.

number of the first shell around the chloride or the sodium ion is calculated as follows

$$N_{ji} = 4\pi\rho_j \int g_{ji}(r) r^2 \mathrm{d}r \qquad (2)$$

where $g_{ji}(r)$ is the radial distribution function of j about i and ρ_j is the bulk number density of j. The hydration number of sodium in hydrate is 5, very close to that in the water phase (5.3). Similarly, the hydration number of the chloride ion in the hydrate and water phases is 6.0 and 6.7, respectively. (Note that our simulation results in the liquid water phase are in good agreement with the values (5.3 for Na^+ and 7.0 for Cl^- in the water phase) from experiment[26] and other simulation data.[27]) Figure 11 shows the hydration number as a function of distance for Na and Cl ions in water and hydrate phases, respectively. It can be seen that the hydration environments are not much different in both phases.

3.3. Cage Structures with the Inclusion of Ions. The existence of ions in the cage structures not only results in the rearrangement of local water structure but also affects the size and shape of water cages and their filling of methane molecules. In the following, we summarize the various types of new water cages that occur upon the inclusion of sodium and chloride ions during the growth of methane hydrates.

3.3.1. Single Chloride Ion Participating in the Cage Structure. We observed two types of crystalline methane hydrates containing a chloride ion: (I) the chloride ion involved in four water cages (Figure 12) and (II) the chloride involved in five water cages (Figure 13). Figure 12 (a) and (b) shows the structure of stacked water cages without and with a chloride ion in type I structure. The chloride ion is surrounded by one 5^{12} cage

dx.doi.org/10.1021/jp308224v | J. Phys. Chem. B 2012, 116, 14115−14125

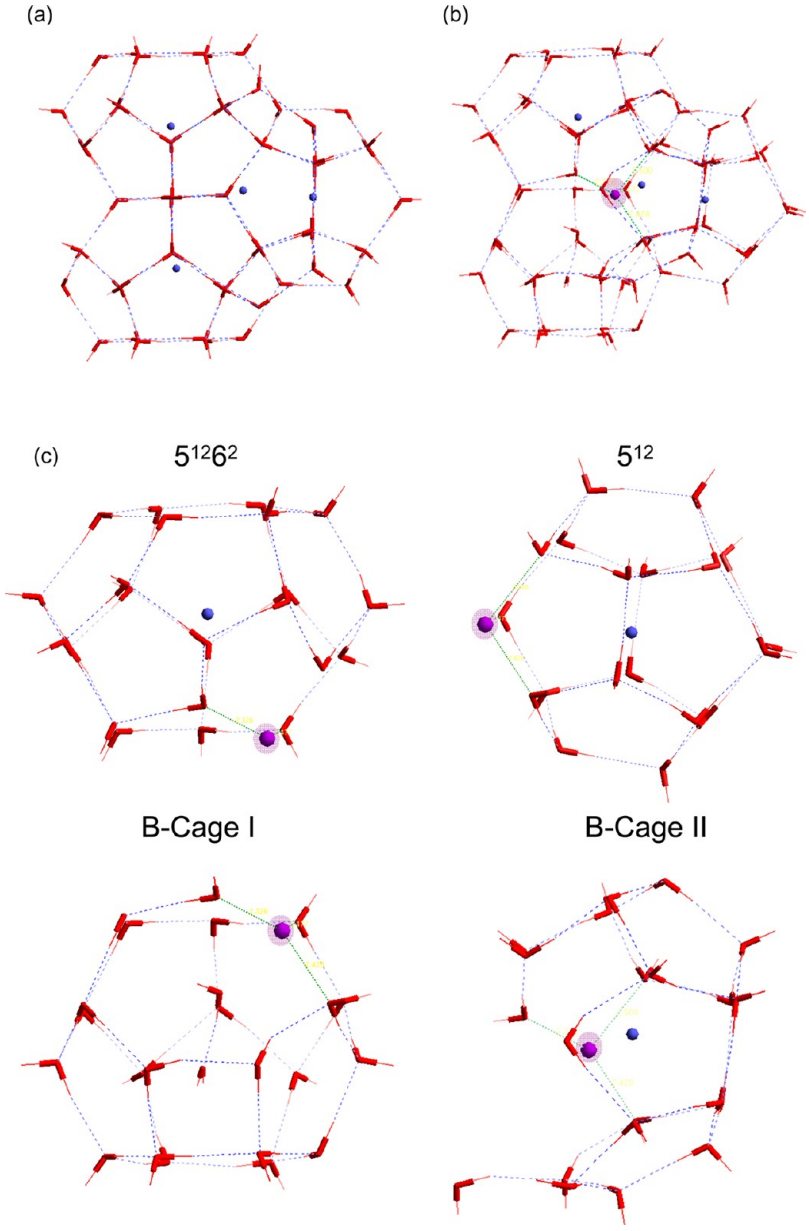

Figure 14. Comparison of the structure of stacked cages without (a) and with (b) the sodium ion. The structure without sodium ions consists of one 5^{12} cage and three $5^{12}6^2$ cages, while one of the $5^{12}6^2$ cages is replaced by B-cage I and the other is replaced by the B-cage II in the structure with the sodium ion (c). The B-cage I is occupied by the water molecules as the guest. The purple and blue balls represent the sodium ions and carbon atoms of methane, respectively. The red cylinder, red stick, and the blue dashed line represent the oxygen and hydrogen atoms of water molecules and the hydrogen bonding.

and three $4^2 5^{10} 6^2$ cages (two rectangles, ten pentagons, and two hexagons) as shown in Figure 12(c), whereas the structure without the chloride ion consists of one 5^{12} cage and three $5^{12}6^2$ cages. The conversion of $5^{12}6^2$ cages to $4^2 5^{10} 6^2$ cages is a result of the replacement of one water molecule by a chloride ion and the displacement of nearby water molecules. The 5^{12} cage expands slightly as one of the water molecules is replaced by a chloride ion. It is noteworthy that the similar hydrogen bonding between the chloride ion and the hydrogen atom of the water molecule is found in the crystalline ice from molecular dynamics simulations of ice growth conducted by Vrbka and Jungwirth.[28]

It is interesting that although a water molecule is hydrogen bonded to four neighboring water molecules in the hydrate phase the chloride ion is hydrated by six water molecules. This is different from the inclusion of a chloride ion in ice where the chloride ion is still hydrated by four, tetrahedrally situated, water molecules.[29] The cavity in the hydrate phase allows for rearrangement of water molecules to better solvate the chloride ion.

Figure 13 shows the structure of stacked cages without and with a chloride ion in the type II structure. In this case, the chloride ion is surrounded by one $4^2 5^{10}$ cage, two $5^{12}6^2$ cages, and two $4^1 5^{12} 6^1$ cages, as shown in Figure 13(c). In other words, the replacement of a water molecule with a chloride ion in this case result in the change of one 5^{12} cage to a $4^2 5^{10}$ cage and two $5^{12}6^2$ cages to $4^1 5^{12} 6^1$ cages. The volume of the $5^{12}6^2$ cage with one chloride ion slightly expands, while those of the $4^2 5^{10}$ and $4^1 5^{12} 6^1$ cages are smaller than the corresponding 5^{12} and $5^{12}6^2$ cages. As a result, we found that the methane molecule does not enter into $4^2 5^{10}$ or $4^1 5^{12} 6^1$ cages. In this case, the occupancy of methane in

dx.doi.org/10.1021/jp308224v | J. Phys. Chem. B 2012, 116, 14115−14125

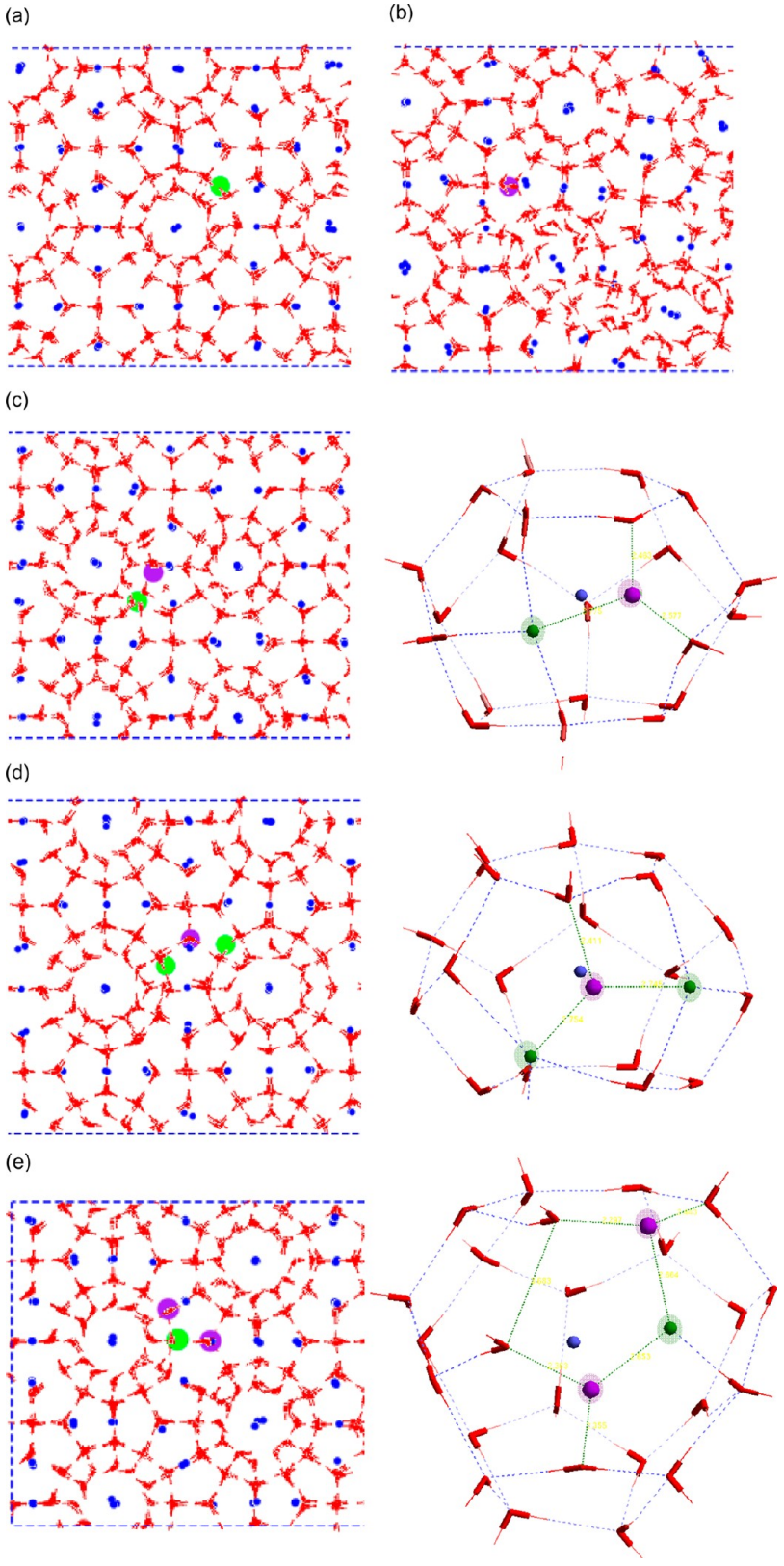

Figure 15. Single negatively charged chloride (a) or positively charged sodium ion (b) included in the structure of stacked cages. The three types of both chloride and sodium ions into the structure of stacked cages and their related cages are also shown in (c)~(e). The green, purple, and blue balls represent the chloride ions, sodium ions, and carbon atoms of methane, respectively.

the cavity of the hydrate phase is reduced due to the inclusion of chloride ions in the hydrate phase.

3.3.2. Single Sodium Ion Participating in the Cage Structure. Figure 14(a) and (b) shows the structure of stacked cages without and with a sodium ion. In this case, the sodium ion is involved in four cages: one 5^{12} cage, one $5^{12}6^2$ cage, and two broken cages, referred to as B-cage I and B-cage II, respectively (Figure 14(c)). Without the sodium ion, the structure consists of

dx.doi.org/10.1021/jp308224v | *J. Phys. Chem. B* 2012, 116, 14115−14125

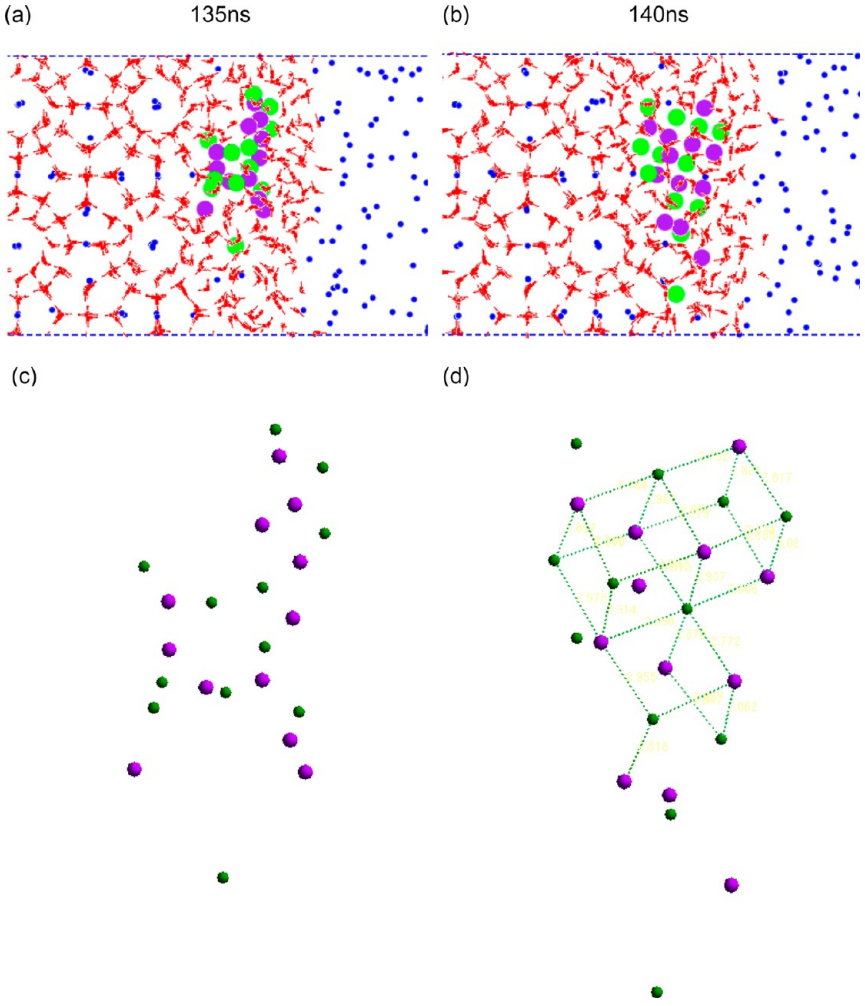

Figure 16. Snapshots of the model near the end (135 and 140 ns) of our simulations. The chloride and sodium ions are confined in a small region of liquid water, (a) and (c). The chloride and sodium ions begin to arrange regularly according to the sodium chloride crystal lattice as shown in (b) and (d).

one 5^{12} cage and three $5^{12}6^2$ cages. The sodium ion has a significant influence on the water arrangement in the B-cages. First, one additional water in B-cage I is pulled nearby the sodium ion (such that its hydration number is increased to 5). This displaced water molecule attracts another water molecule to move to the cavity of B-cage I. As a result, these two water molecules appear to be the guest molecules in B-cage I, and the methane molecule no longer occupies this cage. Note that a similar defect (water serves as a guest molecule) is reported by Vatamanu and Kusalik in the growth of methane hydrate in the system without ions.[13a] The significant structure change of B-cage I also results in the defects in its neighboring B-cage II. As can be seen in Figure 15(b), there are many structure defects in the hydrate phase near the sodium ion.

3.3.3. Chloride and Sodium Ion Pairs Participating in the Cage Structure. In our simulations, we also observe cases where chloride and sodium ion pairs are included in the crystalline structure of methane hydrate. There are three types of such inclusions: (1) one NaCl pair (Figure 15(c)), (2) one NaCl pair plus one chloride ion (Figure 15(d)), and (3) one NaCl pair plus one sodium ion (Figure 15(e)). In addition to the favorable Coulomb interactions between sodium and chloride ions, the similar equilibrium separation distance of NaCl in its crystal lattice (2.83 Å) and that of oxygen atoms in the hydrate phase (2.75 Å) may facilitate the inclusion of NaCl pairs into the hydrate structure.

3.4. Precipitation of Salt from the Growth of Crystalline Hydrate. During the growth of methane hydrate, the concentration of sodium chloride in the liquid phase increases and eventually precipitates, as shown in Figure 16. In the final stage of growth, the chloride and sodium ions are constrained in the small region where a few liquid water molecules remain (Figure 16(a) and (c)). At 140 ns, the chloride and sodium ions begin to arrange regularly according to the sodium chloride crystal lattice (Figures 16(b) and (d)). In this region where the solid sodium chloride crystallizes, none of the water molecules exist. The distance between the sodium and chloride ions of the sodium chloride crystal obtained from our simulation is measured to be close to the experiment value 2.83 Å.

4. CONCLUSION

We successfully perform the molecular dynamics simulations for studying the growth and dissociation of CH_4 hydrates with sodium chloride present in the liquid phase by using the three-phase molecular models. The equilibrium temperatures of CH_4 hydrate for the system containing sodium chloride aqueous solution are found to be lower than that obtained from the system without sodium chloride by about 2−3 K, in good agreement with experiments. We also studied the effect of sodium chloride ions on the growth rate of CH_4 hydrate. The growth rates of methane hydrates in sodium chloride aqueous

dx.doi.org/10.1021/jp308224v | J. Phys. Chem. B 2012, 116, 14115−14125

solution are found to be lower than that in pure water. The main reason for the reduced growth rate of methane hydrate is the slowed water repelling process in the growing layer due to the hydration of charged species located near the solid−liquid interface. The ions can be included in the water network in the hydrate phase by replacing the water molecules. The presence of ions in the hydrate phase leads to locally distorted water cages. The cavity of the distorted cages nearby the ions may become too small to accommodate methane molecules or contain water molecules as guest. As a result, the occupancy of methane is reduced in the case of growth of hydrate in NaCl aqueous solutions compared to that in pure water.

AUTHOR INFORMATION

Corresponding Author

*E-mail stlin@ntu.edu.tw.

Notes

The authors declare no competing financial interest.

ACKNOWLEDGMENTS

The author would like to thank the financial support from Grants 100-5226904000-02-04 and 101-5226904000-06-03 by the Ministry of Economic Affairs of Taiwan and computation resources from the National Center for High-Performance Computing of Taiwan and Computer and Information Networking Center of National Taiwan University.

REFERENCES

(1) (a) Sloan, E. D.; Carolyn, A. K. *Clathrate hydrates of natural gases*, 3rd ed.; CRC Press: London, 2008. (b) Sloan, E. D. *Nature* **2003**, *426* (6964), 353−359.

(2) (a) Dickens, G. R.; Paull, C. K.; Wallace, P. *Nature* **1997**, *385* (6615), 426−428. (b) Gornitz, V.; Fung, I. *Global Biogeochem Cycles* **1994**, *8* (3), 335−347. (c) Haq, B. U. *Science* **1999**, *285* (5427), 543−544. (d) Kvenvolden, K. A. *Rev. Geophys.* **1993**, *31* (2), 173−187.

(3) (a) Tung, Y. T.; Chen, L. J.; Chen, Y. P.; Lin, S. T. *J. Phys. Chem. B* **2010**, *114* (33), 10804−10813. (b) Tung, Y. T.; Chen, L. J.; Chen, Y. P.; Lin, S. T. *J. Phys. Chem. C* **2011**. (c) Anderson, B. J.; Tester, J. W.; Borghi, G. P.; Trout, B. L. *J. Am. Chem. Soc.* **2005**, *127* (50), 17852−17862. (d) Jacobson, L. C.; Hujo, W.; Molinero, V. *J. Am. Chem. Soc.* **2010**, *132* (33), 11806−11811. (e) Moon, C.; Taylor, P. C.; Rodger, P. M. *J. Am. Chem. Soc.* **2003**, *125* (16), 4706−4707. (f) Vatamanu, J.; Kusalik, P. G. *J. Am. Chem. Soc.* **2006**, *128* (49), 15588−15589. (g) Walsh, M. R.; Koh, C. A.; Sloan, E. D.; Sum, A. K.; Wu, D. T. *Science* **2009**, *326* (5956), 1095−1098. (h) Nada, H. *J. Phys. Chem. B* **2006**, *110* (33), 16526−16534. (i) English, N. J.; Phelan, G. M. *J. Chem. Phys.* **2009**, *131* (7), 074704. (j) Forrisdahl, O. K.; Kvamme, B.; Haymet, A. D. J. *Mol. Phys.* **1996**, *89* (3), 819−834.

(4) (a) Deroo, J. L.; Peters, C. J.; Lichtenthaler, R. N.; Diepen, G. A. M. *AIChE J.* **1983**, *29* (4), 651−657. (b) Jager, M. D.; Sloan, E. D. *Fluid Phase Equilib.* **2001**, *185* (1−2), 89−99. (c) Seo, Y.; Lee, H. *J. Phys. Chem. B* **2003**, *107* (3), 889−894. (d) Richon, D.; Mohammadi, A. H.; Afzal, W. *J. Chem. Thermodyn.* **2008**, *40* (12), 1693−1697.

(5) Qi, Y. X.; Wu, W. D.; Liu, Y. F.; Xie, Y. M.; Chen, X. *Fluid Phase Equilib.* **2012**, *325*, 6−10.

(6) Kelland, M. A. *Energy Fuels* **2006**, *20* (3), 825−847.

(7) Wu, M.; Wang, S.; Liu, H. *J. Nat. Gas Chem.* **2007**, *16* (1), 81−85.

(8) Del Villano, L.; Kommedal, R.; Fijten, M. W. M.; Schubert, U. S.; Hoogenboom, R.; Kelland, M. A. *Energy Fuels* **2009**, *23* (7), 3665−3673.

(9) Bernal, J. D.; Fowler, R. H. *J. Chem. Phys.* **1933**, *1* (8), 515−548.

(10) *Cerius2*; Molecular Simulations Inc.: San Diego, 1999.

(11) Jorgensen, W. L.; Chandrasekhar, J.; Madura, J. D.; Impey, R. W.; Klein, M. L. *J. Chem. Phys.* **1983**, *79* (2), 926−935.

(12) Jorgensen, W. L.; Maxwell, D. S.; TiradoRives, J. *J. Am. Chem. Soc.* **1996**, *118* (45), 11225−11236.

(13) (a) Vatamanu, J.; Kusalik, P. G. *J. Phys. Chem. B* **2006**, *110* (32), 15896−15904. (b) Vatamanu, J.; Kusalik, P. G. *J. Phys. Chem. B* **2008**, *112* (8), 2399−2404.

(14) Chandrasekhar, J.; Spellmeyer, D. C.; Jorgensen, W. L. *J. Am. Chem. Soc.* **1984**, *106* (4), 903−910.

(15) Aqvist, J. *J. Phys. Chem.* **1990**, *94* (21), 8021−8024.

(16) Kim, J. S.; Yethiraj, A. *J. Chem. Phys.* **2008**, *129* (12), 124504.

(17) (a) Cao, Z. T.; Tester, J. W.; Sparks, K. A.; Trout, B. L. *J. Phys. Chem. B* **2001**, *105* (44), 10950−10960. (b) Cao, Z. T.; Tester, J. W.; Trout, B. L. *J. Chem. Phys.* **2001**, *115* (6), 2550−2559.

(18) Steve, P.; Paul, C.; Aidan, T. *Large-Scale Atomic/Molecular Massively Parallel Simulator*; Sandia National Labs: Albuquerque, 2009.

(19) Hoover, W. G. *Phys. Rev. A* **1985**, *31* (3), 1695−1697.

(20) Hoover, W. G. *Phys. Rev. A* **1986**, *34* (3), 2499−2500.

(21) Melchionna, S.; Ciccotti, G.; Holian, B. L. *Mol. Phys.* **1993**, *78* (3), 533−544.

(22) (a) Darden, T.; York, D.; Pedersen, L. *J. Chem. Phys.* **1993**, *98* (12), 10089−10092. (b) Hockney, R. W.; Eastwood, J. W. *Computer Simulation Using Particles*; Adam Hilger: New York, 1989. (c) Pollock, E. L.; Glosli, J. *Comput. Phys. Commun.* **1996**, *95* (2−3), 93−110.

(23) (a) English, N. J.; MacElroy, J. M. D. *J. Chem. Phys.* **2004**, *120* (21), 10247−10256. (b) English, N. J.; Johnson, J. K.; Taylor, C. E. *J. Chem. Phys.* **2005**, *123* (24), 244503. (c) Hawtin, R. W.; Quigley, D.; Rodger, P. M. *Phys. Chem. Chem. Phys.* **2008**, *10* (32), 4853−4864. (d) Myshakin, E. M.; Jiang, H.; Warzinski, R. P.; Jordan, K. D. *J. Phys. Chem. A* **2009**, *113* (10), 1913−1921. (e) Fidler, J.; Rodger, P. M. *J. Phys. Chem. B* **1999**, *103* (36), 7695−7703.

(24) Baez, L. A.; Clancy, P. *Ann. N. Y. Acad. Sci.* **1994**, *715*, 177−186.

(25) (a) Abascal, J. L. F.; Sanz, E.; Fernandez, R. G.; Vega, C. *J. Chem. Phys.* **2005**, *122* (23), 234511. (b) Fernandez, R. G.; Abascal, J. L. F.; Vega, C. *J. Chem. Phys.* **2006**, *124* (14), 144506. (c) Abascal, J. L. F.; Vega, C. *Phys. Chem. Chem. Phys.* **2007**, *9* (22), 2775−2778.

(26) Ricci, M. A.; Mancinelli, R.; Botti, A.; Bruni, F.; Soper, A. K. *J. Phys. Chem. B* **2007**, *111* (48), 13570−13577.

(27) (a) Smith, E. J.; Bryk, T.; Haymet, A. D. J. *J. Chem. Phys.* **2005**, *123*, 3. (b) Marcus, Y. *Chem Rev* **2009**, *109* (3), 1346−1370.

(28) (a) Vrbka, L.; Jungwirth, P. *Phys. Rev. Lett.* **2005**, *95* (14), 148501. (b) Jungwirth, P.; Vrbka, L. *J. Mol. Liq.* **2007**, *134* (1−3), 64−70.

(29) Feibelman, P. J. *Phys. Rev. B* **2007**, *75* (21), 214113.